Proceedings of ASME Turbo Expo 2011
GT2011
June 6-10, 2011, Vancouver, British Columbia, Canada

GT2011-46757

OPTIMIZATION OF AN AXIAL TURBINE ROTOR FOR HIGH AERODYNAMIC INLET BLOCKAGE

Mohammad Arabnia † **Vadivel K. Sivashanmugam** ‡ **Wahid Ghaly**§ *
Department of Mechanical and Industrial Engineering
Concordia University
Montreal,QC, H3G 1M8
Canada

ABSTRACT

This paper presents a practical and effective optimization approach to minimize 3D-related flow losses associated with high aerodynamic inlet blockage by re-stacking the turbine rotor blades. This approach is applied to redesign the rotor of a low speed subsonic single-stage turbine that was designed and tested in DLR, Germany. The optimization is performed at the design point and the objective is to minimize the rotor pressure loss coefficient as well as the maximum von Mises stress while keeping the same design point mass flow rate, and keeping or increasing the rotor blade first natural frequency. A Multi-Objective Genetic Algorithm (MOGA) is coupled with a Response Surface Approximation (RSA) of the Artificial Neural Network (ANN) type. A relatively small set of high fidelity 3D flow simulations and structure analysis are obtained using ANSYS Workbench Mechanical. That set is used to train and to test the ANN models. The stacking line is parametrically represented using a quadratic rational Bezier curve (QRBC). The QRBC parameters are directly related to the design variables, namely the rotor lean and sweep angles and the bowing parameters. Moreover, it results in eliminating infeasible shapes and in reducing the number of design variables to a minimum while providing a wide design space for the blade shape. The aero-structural optimization of the E/TU-3 turbine proved successful, the rotor pressure loss coefficient was reduced by 9.8% *and the maximum von Mises stress was reduced by* 36.7%*. This improvement was accomplished with as low as four design variables, and is attributed to the reduction of 3D-related aerodynamic losses and the redistribution of stresses from the hub trailing edge region to the suction side maximum thickness area. The proposed parametrization is a promising one for 3D blade shape optimization involving several disciplines with a relatively small number of design variables.*

Nomenclature

b	Blockage = $\frac{\int_A (u/U) dA}{\int_A dA}$
C_p	Pressure coefficient
f_1	Blade 1^{st} natural frequency
$\dot{m}$	Mass flow rate
w	Bowing intensity
Y	Pressure loss coefficient = $\frac{P_{t,in}-P_{t,out}}{P_{t,in}-P_{out}}$

Greek symbols

α	Blade lean angle (degree)
β_r	Blade sweep angle (°)
$\beta_{1,2}$	Relative flow angle (°)
γ	Blade span ratio
σ	Stress
ω	Rotation speed

Subscripts

$1,2$	Rotor inlet, outlet
$0,t$	Total (or stagnation)
a	Aerodynamic

*†m_arabni@encs.concordia.ca
‡s_vadiv@encs.concordia.ca
§ghaly@encs.concordia.ca (Address all correspondence to this author.)

r	Rotor
s	Structural
vm	von Mises

Acronyms

ANN	Artificial neural network
CFD	Computational fluid dynamics
CSD	Computational structure dynamics
GA	Genetic algorithms
LE, TE	Leading edge, Trailing edge
MDO	Multidisciplinary optimization
$MOGA$	Multi-objective genetic algorithm
$NSGA2$	Non-dominated sorting genetic algorithm
ORG, OPT	Original, optimum
PS, SS	Pressure side, suction side
$QRBC$	Quadratic rational Bezier curve
RBF	Radial basis function
RSA	Response surface approximation
SA	Simulated annealing

1 Introduction

Aero-structural optimization of turbomachinery is of particular importance for the aerospace industry since small improvements in performance can translate into significant savings in operating and manufacturing costs. An automated aero-structural methodology is developed by coupling CFD and CSD simulation tools with optimization algorithms to redesign existing blade shapes for improved performance. Combining two different disciplines in the optimization process increases the complexity of the optimization problem. Moreover the aero-structural optimization is a nonlinear and multimodal problem that could be effectively handled by global optimizers such as Genetic Algorithms (GA) and Simulated Annealing (SA). Many researchers have taken this approach to optimize turbomachinery blading, such as the work given in [1–3].

Shape optimization in three-dimensional flow for turbomachinery was presented by various researchers. Restacking the blade profiles in the spanwise direction can result in significant performance gains. This blade restacking implies the redistribution of the blade lean and sweep. The latter are used extensively; they refer to the translation of the spanwise blade profiles in the tangential and axial directions, respectively. It also implies the change in blade bowing. However, it does not imply any change in blade stagger, which affects rather strongly the stage reaction. Vad [4] has reviewed many papers in this regard and explained the physical effects of sweep and lean, particularly for low-speed axial compressors.

Talya *et al.* [5] and Rajadas *et al.* [6] applied multidisciplinary optimization (MDO) considering aerodynamic, heat transfer, structural and modal objectives to optimize the shape of a generic 3D turbine blade. The blade shape is parameterized using Bezier curves and a constrained multiobjective optimization problem was solved using the Kreisselmeier-Steinhauser (K-S) method. Pierret *et al.* [2, 7] applied GA as optimizer and RBF as a RSA to optimize Rotor 67 by considering aero and structural objectives. The optimization was carried out at several operating points so as to improve the rotor performance over the operating range. A harmonic perturbation-based blade optimization was proposed by Li *et al.* [8], and the methodology was employed to optimize the aero-thermal performance of Rotor 67 by applying mechanical and aero-mechanical constraints. An improvement of 0.4% in isentropic efficiency was reported at the expense of a 33% increase in static stress. Frederic *et al.* [9] developed a fully automated aero-mechanical MDO tool box, which was applied to optimize a high pressure compressor stage to improve its aerodynamic performance subject to mechanical and geometric constraints. The optimization tool contains a NURBS based parametrization scheme and an ANN as the RSA approximation. A differential evolution-based optimization algorithm in combination with a NURBS-based parametrization scheme were developed and applied to optimize Rotor 37 by Luo *et al.* [3].

In the current work, the blade geometry is represented by several two-dimensional sections at different radial locations. They are joined with the stacking curve in the spanwise direction. The stacking curve is parameterized using a Quadratic Rational Bezier Curve (QRBC) [10], whose parameters are related to the blade design variables used in the optimization such as the blade lean, sweep, bowing intensity and radial location. The stacking curve is smooth, with a continuous second order derivative; it can generate a wide range of shapes with a few design parameters without violating any geometrical constraints; it can also be applied in any coordinate system. The main focus of this work is to integrate the aero and structural disciplines in the optimization process so as to decrease three dimensional flow losses and the maximum equivalent blade stress by carefully reshaping the stacking profile.

2 Methodology

In this section, the components of the present optimization methodology are detailed, namely, the shape parametrization QRBC, the optimizer MOGA, the RSA given by ANN, and the optimization objectives.

2.1 Multi-objective genetic algorithm

A real coded NSGA2 is applied to multi-objective optimization by introducing a non-dominated sorting procedure [11]. The initial population is generated randomly within the design space and the fitness in each generation is based on the non-domination level and a niche count factor, which depends on the number and proximity of neighboring solutions. All sets in the first non-domination level are assigned a maximum value of equal dummy fitness and this value may be reduced based on the factor called niche count if that solution is located in the dense region of the solution space. For more details see [11]. The population in the second non-domination level is assigned a dummy fitness, which is smaller than the smallest fitness value of the previous front. The same fitness reduction procedure is carried out based on the niche count. These procedures are repeated until all the individuals are assigned a fitness value. The genetic algorithm operations like selection, crossover, mutation, elitism and reproduction are then carried out on the individuals to provide a search direction towards the Pareto-optimal region and the solution becomes well diversified due to the inclusion of a sharing strategy [11].

2.2 Artificial neural networks

Multi-layer feed forward network is a universal approximation method for any nonlinear continuous function [12], it uses a back propagation algorithm [13]. In the current work, an ANN based RSA model is used to predict the objective functions and constraints, which reduces the computing cost by a factor of about 10 [9, 10]. Building an ANN based RSA model involves two steps: training and testing of the ANN model with a relatively small set of high fidelity CFD and CSD simulation cases. This set is generated at points that are equally distributed in the design space. These points are generated using the Latin Hypercube sampling method [14].

The ANN training/testing process requires a careful selection of parameters, architecture (number of hidden layers and nodes in each layer), transfer function between layers and training strategy. These choices depend on the function being approximated, e.g. the presence of local minima, high problem dimensionality, disparity in input scales, etc. The values used for the aerodynamic and the structure optimization are given later.

2.3 Geometric representation

The blade shape representation is a key factor in the optimization process. The blade geometry is usually obtained by stacking two dimensional airfoils in the spanwise direction usually through their centers of gravity (rotors) or through the leading edge points (stators). Stacking is a leading parameter in controlling the three dimensional flow effects and redistribution of stresses along the blade spanwise direction [15]. This work mainly concentrates on translating the two dimensional sections without altering their shape or orientation with respect to the axial direction. So it was decided to optimize the blade stacking line, in other words, optimize the blade lean, sweep and bowing; this optimization helps also in getting an insight into the design space.

2.3.1 Quadratic rational Bezier curve A QRBC represents exactly a conic curve in an oblique coordinate system, it can be expressed parametrically in terms of $u \in [0,1]$ as [16]:

$$\overrightarrow{C}(u) = \frac{(1-u)^2 w_0 \overrightarrow{P}_0 + 2u(1-u) w_1 \overrightarrow{P}_1 + u^2 w_2 \overrightarrow{P}_2}{(1-u)^2 w_0 + 2u(1-u) w_1 + u^2 w_2} \quad (1)$$

Where $\overrightarrow{C}(u)$ gives the cartesian or cylindrical coordinates of any point on the stacking curve in terms of the parameter u. $\overrightarrow{P}_i$ is the cartesian (or cylindrical) coordinates of control point i. The weight of each control point, w_i, adjusts the slope and the curvature of the curve. The QRBC is a smooth second order curve that represents exactly any conic line, e.g., an ellipse, a parabola, a circle or a hyperbola.

The blade lean, sweep, bowing intensity, and location of the bowing in the radial direction are used as aerodynamic and structural design variables. The design variables are represented in terms of the QRBC parameters namely P_1, P_2, and w_1, so that the design space is identified and the optimum shape is interpreted in terms of the design variables.

2.3.2 Design variables Based on the QRBC representation given in Eq. 1, the QRBC parameters namely, P_i and w_i for $i = 0-2$, can be selected to parameterize the stacking curve. P_0 is fixed at some point on the hub surface (e.g. center of gravity or LE of hub section) and P_2 moves on the tip surface as shown in Fig. 1. In other words, without loss of generality, the coordinates of P_0 and the radial coordinate of P_2 are fixed. Moreover, w_0 and w_2 are set to 1 so that the stacking curve passes through points P_0 and P_2; the axial coordinate of P_1 was chosen to be equal to that of P_0; this choice does not reduce the flexibility of the QRBC to generate a wide variety of shapes for the stacking curve. According to Fig. 1.a, the sweep angle is defined as β and is controlled by the axial coordinate of P_2. Figure 1.b shows the lean angle α, which is set by the circumferential coordinate of P_2. Figure 1.c shows the blade bowing which can be controlled by the circumferential and radial coordinates of P_1 as well as the weight w_1. Therefore the circumferential coordinate of P_1 is fixed and the weight w_1 is chosen as the bowing intensity parameter. The circumferential coordinate of P_1 is specified by the angle $\widehat{P_1 P_0 B}$ as shown in Fig. 1.c and is fixed. The lean angle is positive in the direction of the suction side and the sweep angle is positive in the positive axial direction. With this set up of the QRBC parameters, we end up with 4 design variables per blade row, which are the axial and circumferential locations of P_2, the radial location of P_1, and the weight w_1.

The design variables and their range of variations are first chosen through a parametric study. An important design concern is to keep the design space within a feasible range from a blade structural and manufacturing point of view and, at the same time, be large enough for the optimizer to adequately explore the aero-structural design space. For example bowing the blade creates larger stresses near the hub trailing edge (lowest thickness area) and along the trailing edge at the mid-span section.

2.4 Numerical implementation

2.4.1 Flow analysis The blade shape and computational domain are generated in Gambit (Fluent pre-processor [17]). For each design case, a multi-block structured mesh was generated. The tip clearance is not modeled because the focus is on the stacking curve. The Reynolds-Averaged Navier-Stokes equations have been used to simulate the flow using the second order coupled solver available in Fluent 6.3 and turbulence was modeled using the Spalart-Allmaras model with wall functions where y^+ varies between 30 and 100. The inlet boundary conditions are given as a radial distribution of total pressure and total temperature, two flow angles, the turbulent intensity and hydraulic diameter, whereas the static pressure that would satisfy the radial equilibrium equation is set as the exit boundary condition. Each CFD simulation takes approximately half an hour wall clock time on four CPUs. The flow quantities are averaged, then the total pressure loss coefficient is calculated. The mesh sensitivity analysis suggests $380,000$ cells are adequate for a blade row. The assessment of the numerical calculations with the available experimental data has been discussed in previous work [10].

2.4.2 Structure analysis A static structure analysis was carried out to determine the blade structural stress, displacement and integrity. The CAD geometry for the different turbine blade configurations is modeled in Gambit (Fluent pre-processor [17]) and the geometry cleaning is done in ANSYS ICEMCFD. ANSYS workbench 2.0 Mechanical [18] was used for mesh generation and finite element analysis. Three dimensional solid tetrahedral elements with midside nodes are used to discretize the blade curved profiles. Mesh controlling parameters such as minimum and maximum size of the elements, and growth rate are kept the same for all blade geometries. About 115,000 elements were used to discretize the blade.

In reality, a turbine blade is fitted on the turbine disk therefore it will have a given stiffness value at the hub (blade root) however, in the current work, all the nodes at the blade root are assumed to be fixed so that the blade behaves as a cantilever with zero displacement at the root, which corresponds to the worst case scenario. Compared with compressor blades, turbine blades are normally thicker and heavier due to their operating conditions. The stress resulting from the pressure force is negligible compared to the centrifugal force stress [19]. In this work, the pressure forces are negligible compared to the centrifugal forces, they are neglected when performing the stress analysis, von Mises stress is considered as the main output parameter from

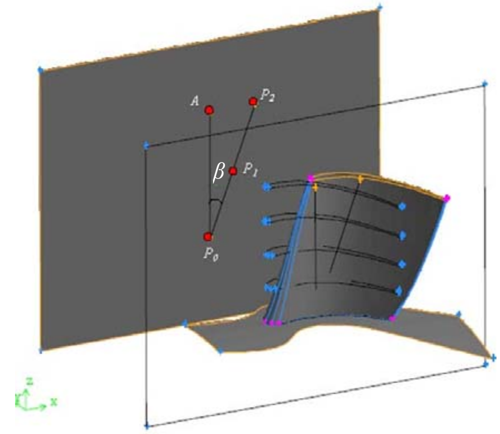

a. swept blade

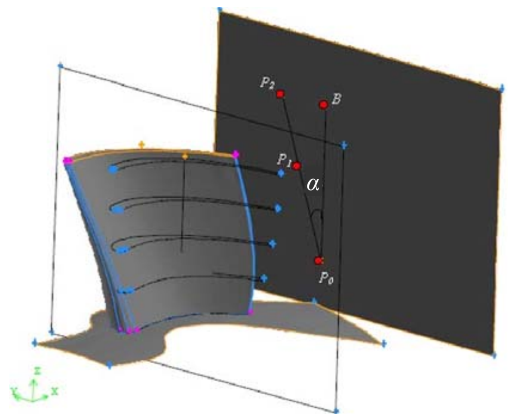

b. leaned blade

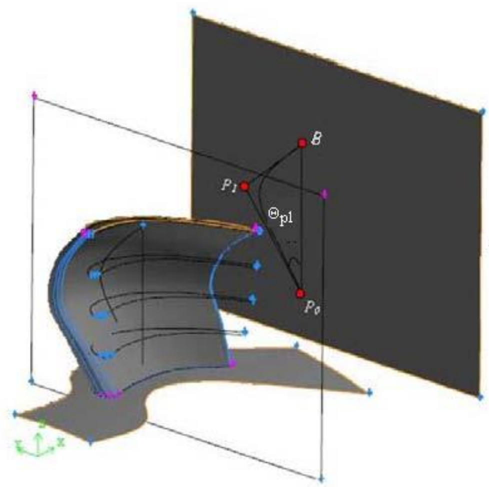

c. bowed blade

Figure 1. Stacking curve parametrization with QRBC

the structural analysis and is used as the structure objective in the aero-structural optimization.

Large tensile stresses that are developed during the blade rotation (due to the centrifugal forces), can be captured by carrying out a static structural analysis. This also causes significant stiffening of the blade. Performing a prestressed modal analysis would provide more realistic values for natural frequencies. Hence, static structure analysis results were taken as an initial guess for the model analysis. ANSYS workbench 2.0 Mechanical option is used to setup the boundary conditions and to calculate the modal frequencies. Note that the modal analysis doesn't require a higher number of elements to calculate the frequencies.

The material used in making the E/TU-3 turbine blade is not available in the literature as the test set up was mainly developed to assess CFD results. Stainless steel is assumed as the blade material, and it has the following properties: elastic modulus $1.93E11$ Pa, Poisson's ratio 0.31, density 7,750 Kg/m^3, tensile yield strength $2.07E8$ Pa, compressive yield strength $2.07E8Pa$ and tensile ultimate yield strength $5.86E8$ Pa.

2.5 Optimization algorithm

A flow chart of the optimization cycle is shown in Fig. 2. The database containing the high fidelity CFD and CSD simulations at the selected sampling points, is developed. It is then used to train and test the ANN models that are used in the optimization loop to evaluate the fitness functions. To improve the prediction capability of the ANN model, database enrichment process has been carried out. During the enrichment process, the optimum candidate obtained at the end of the optimization process is simulated and is included in the database and the ANN is retrained with the updated database, according to the optimization cycle shown in Fig. 2. The database is enriched until the objective predicted by ANN is better than the previous predictions and also the difference between ANN prediction and high fidelity simulation is reduced to an acceptable level.

3 Results and discussion

The E/TU-3 single stage turbine is used as a study-case. It is a well documented, low speed subsonic turbine stage that is built and tested at DLR, Cologne [20]. Its geometry is given as a set of x-, y- and z-coordinates of several 2D airfoil sections located at different spanwise locations from hub to tip. Several geometric and aerodynamic features of that stage are provided in Tables 1 and 2.

The inlet velocity profiles corresponding to different inlet blockages are shown in Fig. 3. These profiles are obtained assuming a $(1/7)^{th}$ velocity profile and the blockage being the displacement thickness given as a percentage of the span. The blockage is considered low when $b < 4\%$, high when $b > 8\%$ and medium when $4\% < b < 8\%$. For the present case, the aero-

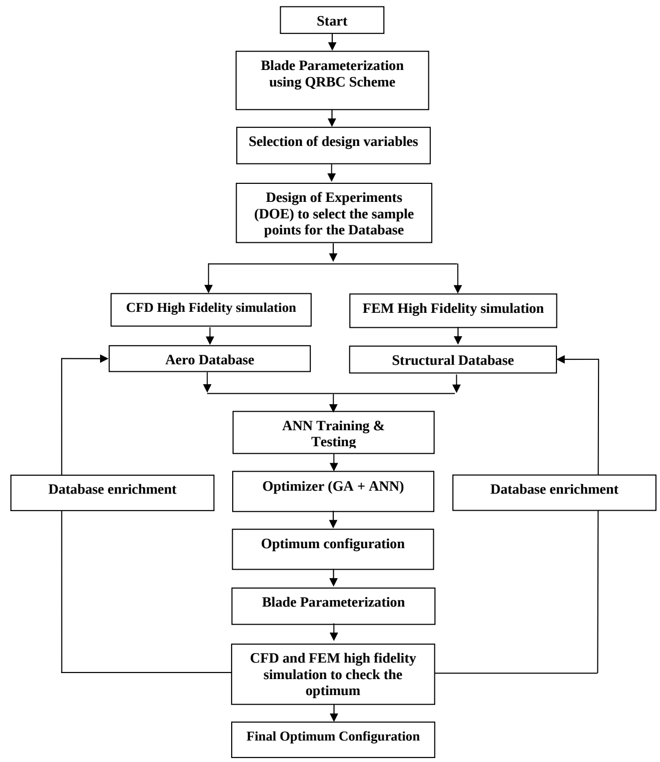

Figure 2. Aero structural optimization cycle

Table 1. E/TU-3 turbine: blade geometry

Data	Stator	Rotor
Number of blades	20	31
Blade aspect ratio	0.56	0.95
Blade solidity	1.56	1.51
Flow deflection	69°	105°

Table 2. E/TU-3 turbine: design point conditions

Inlet total temperature (K)	346
Rotor speed (RPM)	7,800
Stage pressure ratio	0.51
Reynolds number	1.5×10^6
Mid-span flow coefficient	0.74
Mid-span stage loading	1.93
Average reaction (%)	31

dynamic inlet blockage is taken to be b=10%.

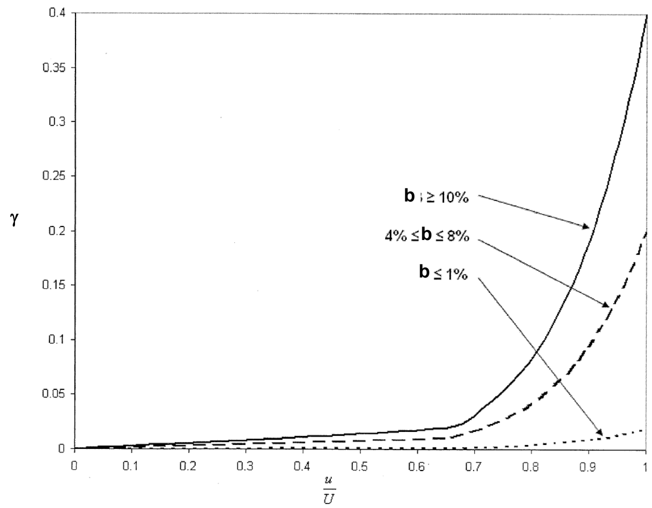

Figure 3. Inlet boundary layer axial velocity profile [21]

The blade stacking line is optimized based on structural and aerodynamic objectives to achieve an overall performance improvement. Optimization is carried out at the design point, i.e. fixed rotor speed, fixed inlet and exit boundary conditions and the mass flow rate is constrained to within 0.5%. The inlet and outlet flow angles were not imposed as constraints. The mean blockage at rotor inlet is considered in this section.

The design parameters are given by the lean angle, sweep angle, the spanwise location of P_1 and the bow intensity, which is controlled by the weight w_1. Geometry candidates are generated by re-stacking the 2D blade sections according to the QRBC representation of the stacking curve, where the QRBC parameters are equally distributed in the design space using the Latin Hypercube method [14].

The optimization objective is a combination of an aerodynamic objective and a structure objective; it is constructed as follows. The pressure loss coefficient is taken as the aerodynamic objective, with mass flow rate as constraint. Von Mises stress is taken as the structural objective and the blade first natural frequency is taken as constraint. The Pareto front is given in Fig. 4.

$$F_{obj}(X) = \{Min(Y_r{}' + PT_a + PT_s), \\ Min(\sigma' + PT_a + PT_s)\} \tag{2}$$

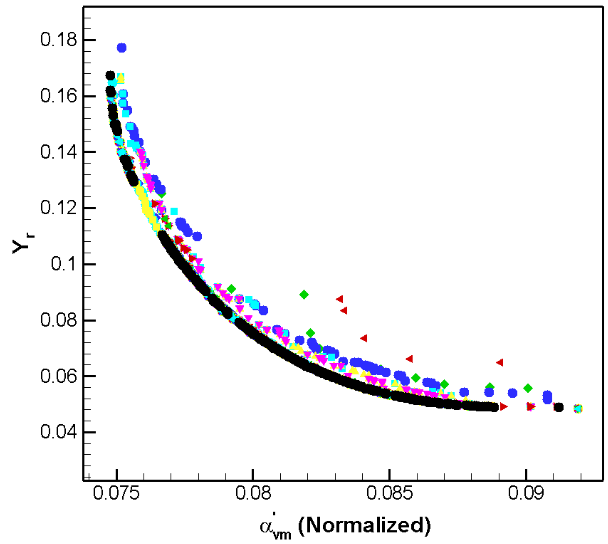

Figure 4. Pareto front: Pressure loss coefficient vs. Normalized von Mises maximum stress

where,

$$PT_a = 0.5 \quad when \quad \frac{|\dot{m} - \dot{m}_{org}|}{\dot{m}_{org}} > 0.005 \\ = 0 \quad otherwise$$

$$PT_s = 0.5 \quad when \quad f_1 < f_{1,org} \\ = 0 \quad otherwise$$

where $f_{1,org} = 2,293$ and, to normalize all individual objectives to be between 0 and 1,

$$f' = \frac{f - f_{min}}{f_{max} - f_{min}} \quad where \quad f = \{Y_r, \sigma\} \tag{3}$$

The ANN models for von Mises stress and natural frequency are trained with the hyperbolic tangent as transfer function because of its asymmetric nature, which were found to perform better in terms of learning and require fewer number of epochs compared with non-symmetric transfer activation functions [22]. Four ANN modules were used to approximate the 4 individual objectives and constraints namely, Y_r, PT_a, σ_{vm} and PT_s. The number of training and testing patterns were chosen to be 90% and 10% for the aerodynamic objectives and 70% and 30% for the structure objectives. The total number of samples in the aerodynamic and structure databases are 27 and 51(initial), respectively. Each GA generation involved 50 individuals and the optimization stops after 150 generations. The value of the mutation and crossover probabilities used were 0.15 and 0.5, respectively. Two elite individuals were selected for passing to the next generation. Because the optimization is done based on the approximate model, the proposed ANN-based optimum design was analyzed with the high fidelity simulations (CFD and CSD).

To improve the ANN model accuracy, database enrichment was implemented. Seven cycles of database enrichment were carried out for the structure discipline as it was found to be the more difficult one to approximate using ANN. Figure 5 shows the converging trend of the discrepancy between the high fidelity (ANSYS) and low fidelity (ANN) results at the end of each enrichment cycle. For the multi-objective optimization process, the ANN model obtained from the enrichment process was selected.

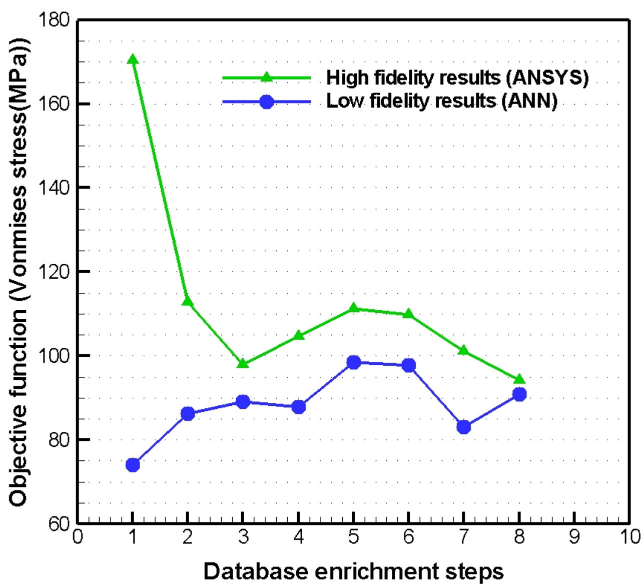

Figure 5. Database enrichment for the structure discipline

3.1 Aerodynamic performance improvement

The original and optimized blade shapes are shown in Fig. 6. The optimized blade is swept backwards by 2.1° and is leaned towards the blade SS by 11.8°, and the blade bowing is zero (straight stacking line). The bowing intensity is zero as a compromise between the aerodynamic and the structure objectives. Note that, if the structure objective is ignored, the bowing parameter is non zero so as to reduce the secondary flow losses associated with the inlet blockage. For the optimized rotor, the pressure loss coefficient decreased from 0.1854 to 0.1670, a decrease of 9.8%, see Table 3.

Table 3. Multi-objective aero-structural optimization: Optimum design variables, objectives and constraints

Case	α_r°	β_r°	γ	w_1	Y_r	σ_{vm} $[MPa]$	f_1 $[s^-1]$	$\dot{m}$ $[kg/s]$
ORG.	0	0	0	0	0.1854	176	2,293	0.320
OPT.	11.8	2.1	0.8	0.0	0.1670	111	2,460	0.321
min	-5	-10	0.2	0	–	–	–	–
max	20	15	0.8	3	–	–	–	–

The blade lean and sweep affect rather strongly the blade spanwise loading and mass flux distributions. In general, leaning towards the blade suction side will unload the tip and put more load at hub and vice versa. The spanwise variation of relative inlet and exit flow angles, shown in Fig. 7.a, indicates a decreased flow turning ($\beta_1 - \beta_2$) between hub and 40% span and an increased turning between 40% span and tip. For the optimized blade, the inlet flow angle suggests a smaller incidence angle near the hub. The spanwise variation of mass flux, depicted in Fig. 7.b, suggests that the optimized blade shape results in less spanwise flow migration particularly in the hub region. Figure 7.c shows a reduction in the optimized radial mass flux which implies a reduced secondary velocity and hence a more uniform flow at exit.

The spanwise pressure loading distribution is indicated in Fig. 8, where the tip loading is higher than the hub loading. The pressure loading decreased at the tip and increased at the hub, see Figs. 8.a and 8.c. These results are consistent with the changes in blade lean and sweep between the original and the optimized blade profiles.

3.2 Structure improvement

For medium and high aerodynamic blockage, an increase in the blade bowing would result in a reduction in secondary flow losses. However, from a structural point such an increase would also result in an increase in the maximum von Mises stress. These competing effects may explain the fact that the optimized blade is straight (the bowing intensity is zero) and proves the robustness of the optimizer scheme. Figures 9, 10, and 11 compare the von Mises stress distribution for the original and optimized configurations. For comparison purposes, the same range of values and stress levels are maintained for all stress contours. In the original configuration the maximum stress occurs at the blade root near TE, where the lowest blade thickness is located

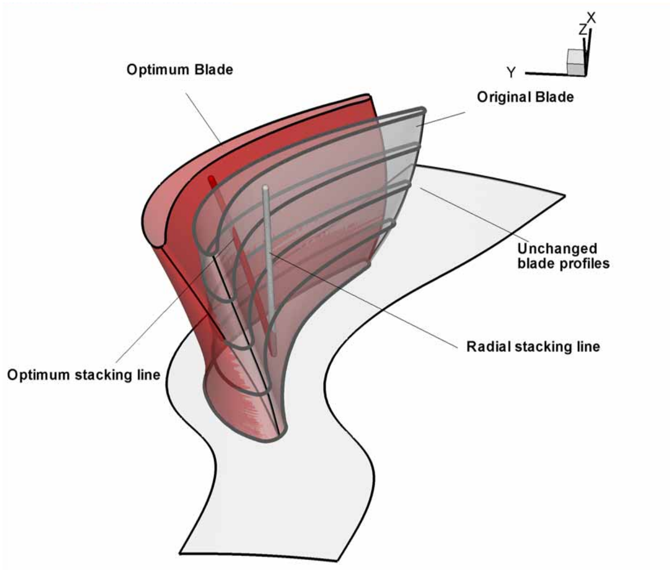

Figure 6. Original and optimum blade shapes

Table 4. Original and optimum blade structure

Case	σ_{vm} $[MPa]$	% Change	f_1 $[s^-1]$	% Change
Original	176		2293	
		36.7		7.28
Optimum	111		2460	

whereas for the optimum configuration, the maximum stress occurs on the SS near the hub where the maximum thickness area is located. Large tensile forces developed due to centrifugal forces tend to straighten the blade and also result in an increase in stress levels at the root. Modification of the stacking line profile resulted in a reduction of the maximum von Mises stress from 176 MPa to 111 MPa, a 36.7% reduction.

The optimum blade has a combined lean and sweep with zero bow, which modifies the center of mass as well as the tangential and axial moments. A change in lean and sweep increases the tangential moment and these changes in structural loading are effectively handled by the available blade thickness distribution along the span. Moreover the shift in center of mass along with the change in moments reduce the trailing edge untwisting effect and result in reducing the maximum stress by 36.73% compared to the von Mises stress on the original blade. The original and optimum stress values are compared in Table 4.

The location of the maximum stress (with less intensity) also shifts from the hub TE location to the SS maximum thickness

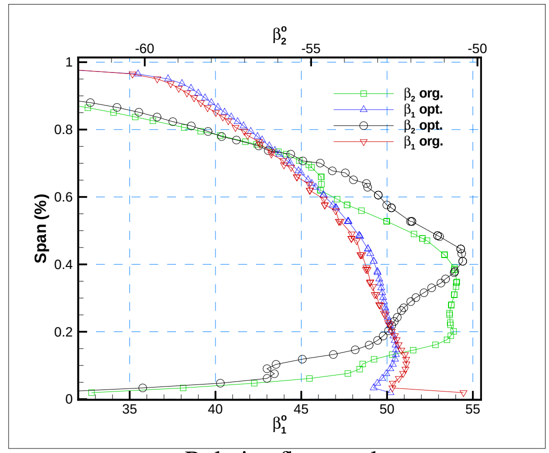

a. Relative flow angle

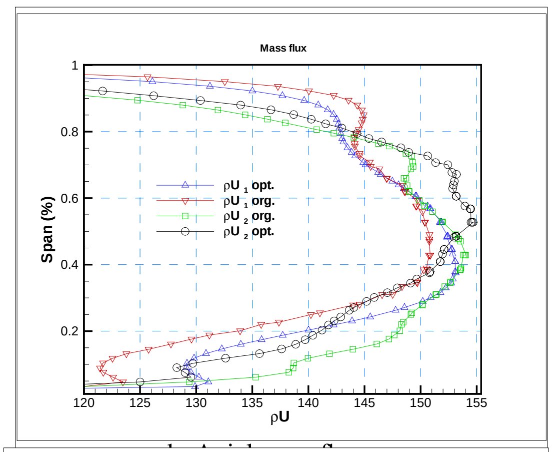

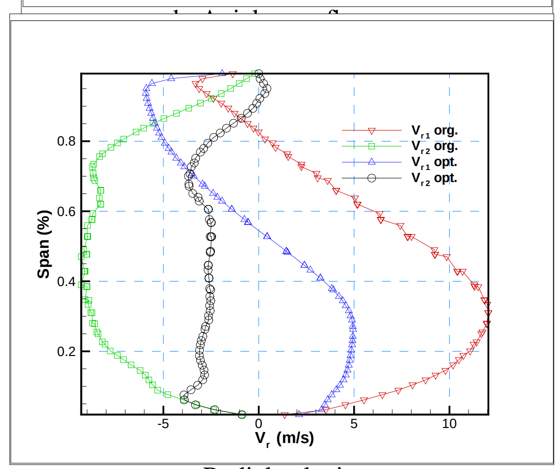

c. Radial velocity

Figure 7. Radial distribution of (a) the relative flow angle, (b) the axial mass flux and (c) the radial velocity near the LE (1) and the TE (2)

Table 5. Surface-based comparison of von Mises stress (MPa) at hub, PS and SS for the original and optimum blades

Surface	*Original*	*Optimum*
Hub	7.2849	6.426
PS	5.93	5.7413
SS	6.1425	10.652

location Fig.11, and the TE is no longer a critical stress location. To understand the overall effect of lean and sweep, von Mises stress has been averaged on the PS, SS and hub surfaces using ANSYS APDL programming and the averaged values are given in Table 5. Due to lean, the average von Mises stress on the blade suction side increases by 73% but this is effectively handled by the available spanwise distribution of the blade thickness. Hence the average stress on the hub surface and on the PS decreased by 12% and 3% respectively. It should be noted that the E/TU-3 turbine is a low speed turbine, $RPM = 7,800$, compared to current high speed turbine stages, for which the stress reductions would be more significant.

4 Conclusion

The aero-structural optimization of a low speed turbine rotor blade was successfully carried out in the presence of a 10% aerodynamic inlet blockage; the design variable being the stacking line. The rotor redesign was carried out at the design point and resulted in reducing the pressure loss coefficient by 9.8% and the maximum von Mises stress by 36.7%. These improvements are due to the reduction in three dimensional flow losses while redistributing the blade stresses through the variation of lean and sweep. The optimized blade turned out to be straight in the spanwise direction. The blade design variables namely lean, sweep and bowing are directly related to the QRBC parametrization of the stacking line and reduce to only 4 design variables controlling the blade shape. The proposed MDO scheme is attractive as it is modular and can couple several disciplines in a multi-stage turbine (or compressor) as it involves 4 design variables per blade row.

REFERENCES

[1] Oyama, A., Liou, M., and Obayashi, S., 2002. "Transonic axial flow blade shape optimization using evolutionary algorithm and three dimensional naviers-stokes solver". *AIAA Paper 2002-5642*.

[2] Pierret, S., Filomeno Coelho, R., and Kato, H., 2007. "Multidisciplinary and multiple operating points shape optimization of three dimensional compressor blades". *Journal of Structure and Multidisciplary optimization, 33(1):61-70*.

[3] Luo, C., Song, L., Li, J., and Feng, Z., 2009. "Multiobjective optimization approach to multidisciplinary design of a three dimensional transonic compressor blade". *Proceedings of Turbo Expo 2009, GT2009-59982*.

[4] Vad, J., 2008. "Aerodynamics effects of blade sweep and skew in low-speed axial flow rotors at the design flow rate: an overview". *Journal of Power and Energy,* ***Vol. 222, Number 1/2008***, pp. 69–85.

[5] Talya, S., Chattopadhyay, A., and Rajadas, J., 2000. "Multidisciplinary analysis and design optimization procedure for cooled gas turbine blades". *8th AIAA/USAF/NASA/ISSMO Symposium on Multidisciplinary Analysis and Optimization, AIAA-2000-4877*.

[6] Rajadas, J., and Chattopadhyay, A., 2002. "Application of design optimization to turbomachinery desgin". *9th AIAA/ISSMO Symposium on Multidisciplinary Analysis and Optimization, AIAA-2002-5662*.

[7] Pierret, S., 2005. "Multi-objective and multi-disciplinary optimization of three-dimensional turbomachinery blades". *6th World Congress of Structural and Multidisciplinary optimization, 30 May - 03 June 2005, Brazil*.

[8] Li, H.-D., He, L., Li, Y., and Wells, R., 2006. "Blading aerodynamics design optimization with mechanical and aeromechanical constraints". *Proceedings of Turbo Expo 2006, GT2006-90503*.

[9] Pouzadaoux, F., Reydellet, G., Taillefer, E., and Masmoudi, M., 2008. "Introduction of multi-disciplinary optimization in compressor blade desig.". *12th AIAA/ISSMO Multidisciplinary Analysis and Optimization Conference, AIAA 2008-6018*.

[10] Arabnia, M., and Ghaly, W., 2009. "A strategy for multi-point shape optimization of turbine stages in three-dimensional flow". *Proceedings of Turbo Expo 2009, GT2009-59708*.

[11] Deb, K., 2001. *Multi-Objective Optimization using Evolutionary Algorithms*. John Wiley and Sons.

[12] Schalkoff, R., 1997. *Artificial Neural Networks*. McGraw-Hill.

[13] Haykin, S., 1999. *Neural Networks: A Comprehensive Foundation*. 2nd Edition, Prentice-Hall.

[14] McKay, M., Bechman, R., and Conover, W., 1979. "A comparison of three methods for selecting values of input variables in the analysis of output from a computer code". *Technometics,* ***21***(2), pp. 239–245.

[15] Moustapha, H., Zelesky, M. F., Baines, N. C., and Japikse, D., 2003. *Axial and Radial Turbines*. Concepts NREC.

[16] Piegl, L., and Tiller, W., 1995. *The NURBS Book*. Springer.

[17] www.fluent.com.

[18] www.ansys.com. Structural mechanics documentation.

[19] Hill, P., and Peterson, C., 1992. *Mechanics and Thermody-*

namics of Propulsion. 2nd Edition, Addison-Wesley Publishing Company.

[20] Fottner, L., 1990. “Test cases for computation of internal flows in aero engine components”. *AGARD-AR-275*. Propulsion and Energetics Panel.

[21] Farber, S., 2008. “Pressure loss modeling of non-symmetric gas turbine exhaust ducts using cfd”. Master’s thesis, Concordia University, Mechanical and Industrial Engineering.

[22] Swingler, K., 1996. *Applying Neural Networks A Practical Guide*. Acdemic Press.

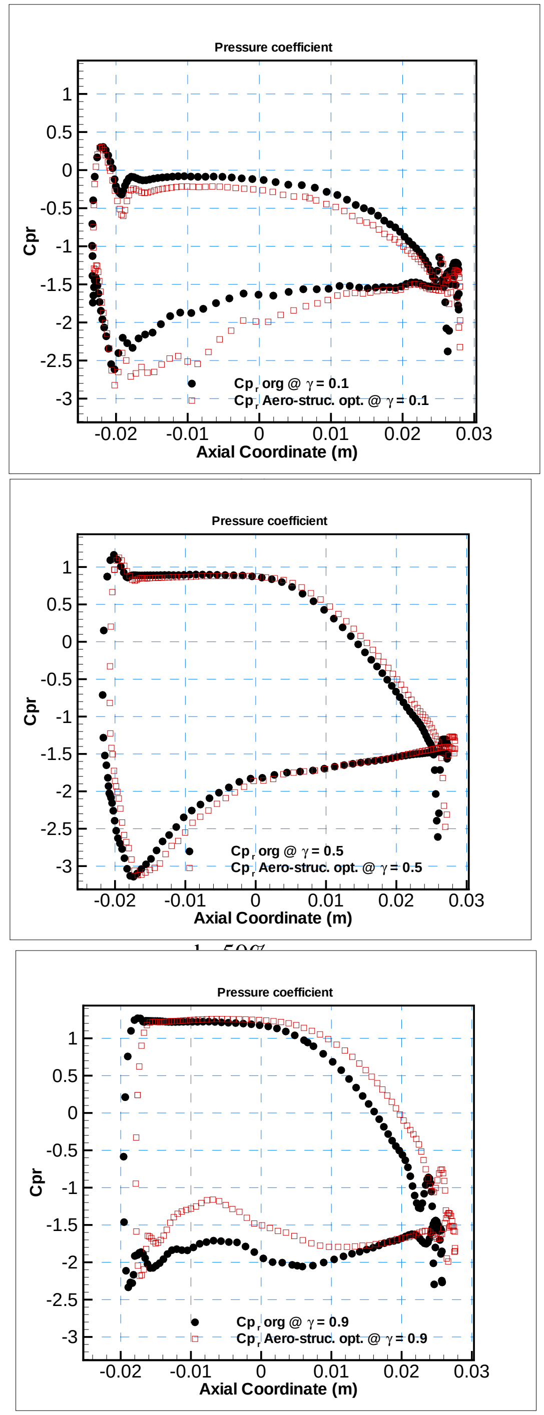

c. 90% span

Figure 8. Rotor blade pressure distribution at hub, mid-span and tip

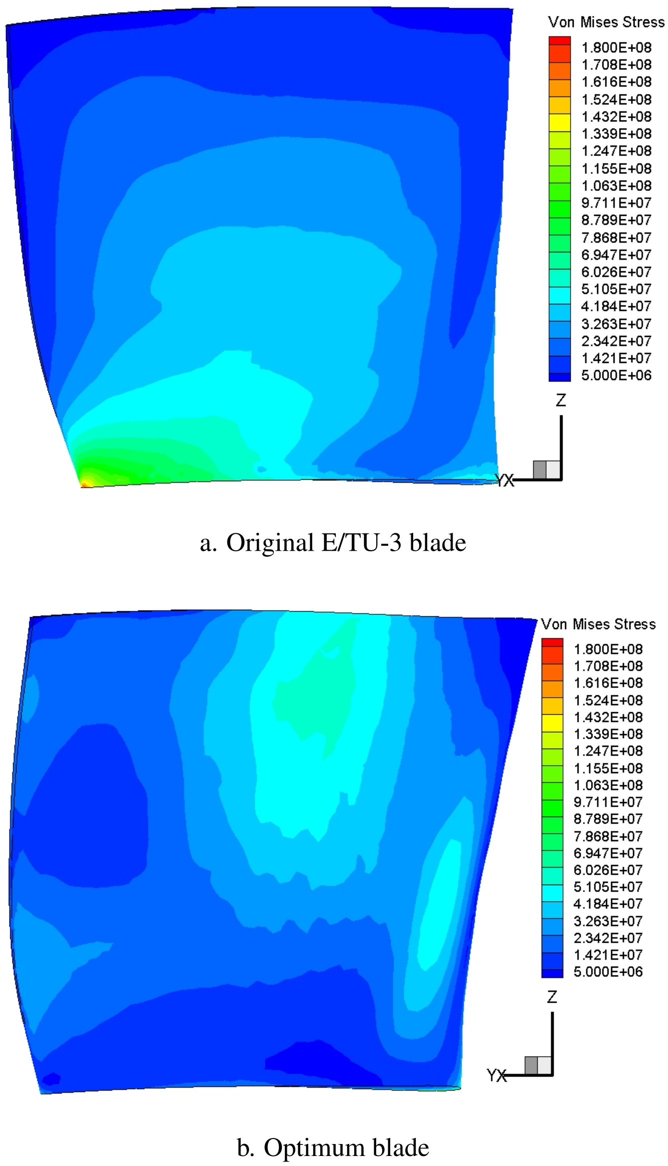

Figure 9. Stress contours on the pressure surface

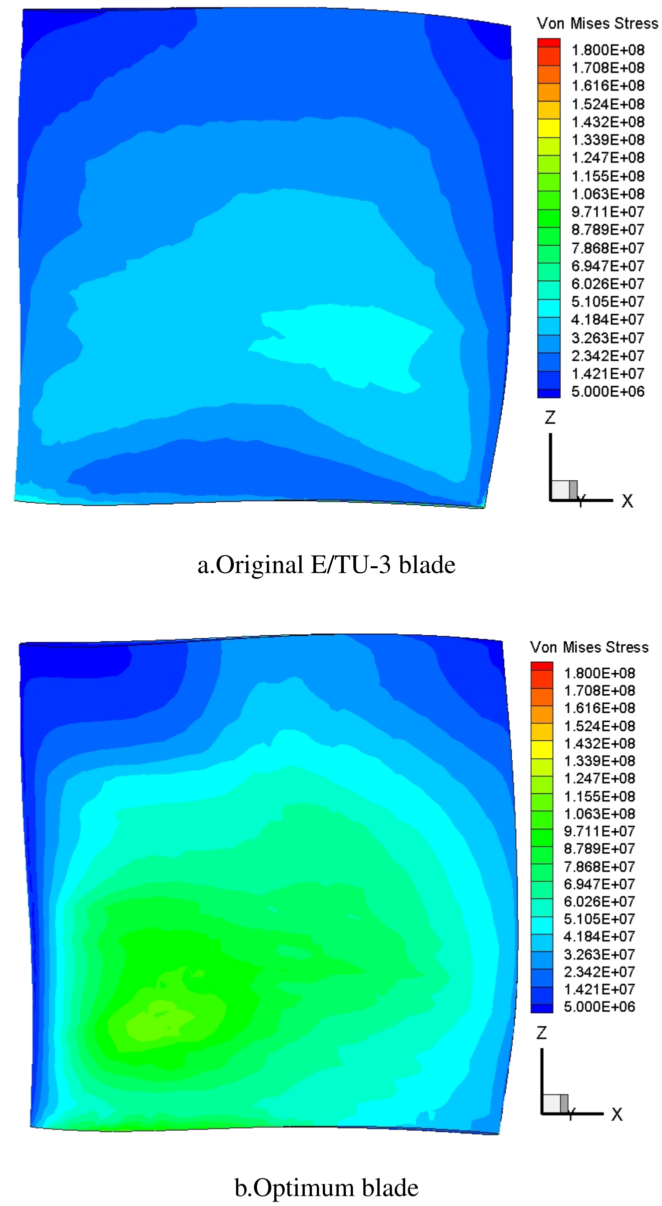

Figure 10. Stress contours on the suction surface

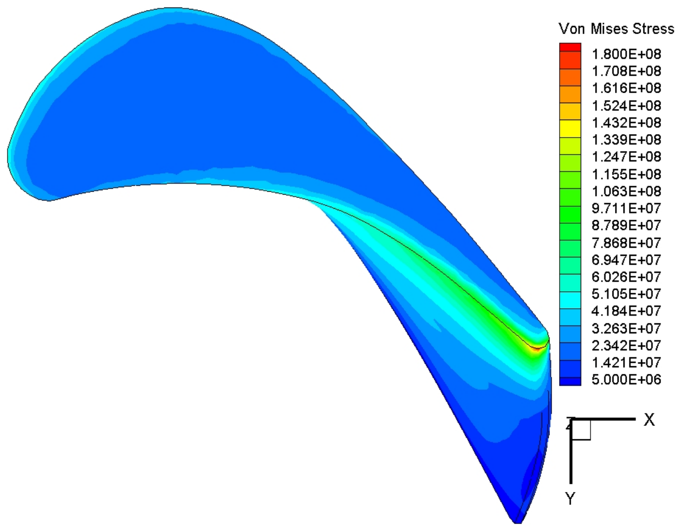

a.Original E/TU-3 blade

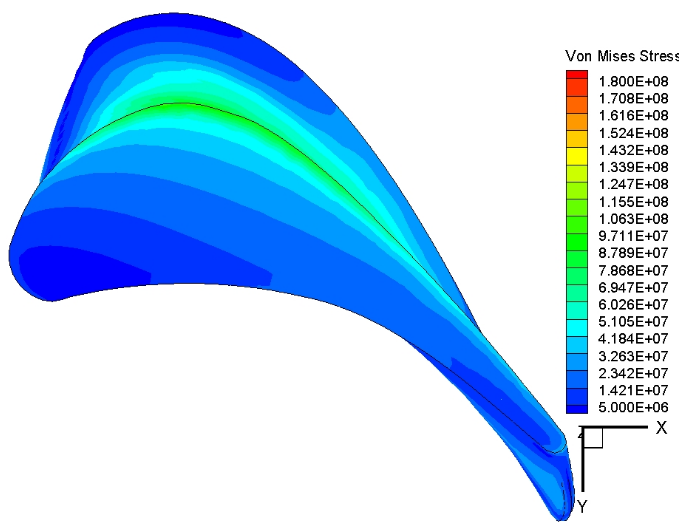

b.Optimum blade

Figure 11. Stress contours on the hub surface